Multiphysics Modeling and Simulation of 3-D Cu–Graphene Hybrid Nanointerconnects

Shuzhan Sun, *Graduate Student Member, IEEE*, and Dan Jiao, *Fellow, IEEE*

***Abstract*— Cu–graphene (Cu-G) hybrid nanointerconnects are promising alternative interconnect solutions for the development of future integrated circuit technology. However, the modeling and simulation of their high-frequency electrical performance remains a challenging problem. To enable the design of complicated Cu-G interconnects, we propose a multiphysics modeling and simulation algorithm to cosimulate Maxwell's equations, dispersion relation of graphene, and Boltzmann equation. We also develop an unconditionally stable time marching scheme to remove the dependence of time step on space step for an efficient simulation of the multiscaled and multiphysics system. Extensive numerical experiments and comparisons with measurements have validated the accuracy and efficiency of the proposed work. This article has also been applied to predict the crosstalk effect and propagation delay of graphene-encapsulated Cu nanointerconnects.**

***Index Terms*— Boltzmann equation, Cu–graphene (Cu-G) hybrid nanointerconnects, finite difference methods, hybrid integrated circuits (ICs), Maxwell's equations, multiphysics modeling and simulation, time-domain analysis, unconditionally stable algorithm.**

I. Introduction

AS INTEGRATED circuits (ICs) have progressed to nanometer-technology nodes and higher levels of integration, existing Cu-based interconnect solution has become increasingly difficult in sustaining the continued evolution of IC technology. Due to side wall and grain boundary scatterings, the resistivity of Cu at small dimensions increases rapidly [1], which leads to, for aggressively scaled Cu interconnects, an increased resistor–capacitor (RC) delay, a lower current-driving capacity, more heat generations, a reduced interconnect bandwidth, a larger crosstalk noise, and other negative effects [2]. As a result, the overall performance and reliability of an IC can degrade significantly.

Cu–graphene (Cu-G) hybrid nanointerconnect solutions, such as graphene-encapsulated Cu interconnects, are promising alternatives to Cu-based interconnects. The hybrid can benefit from the combined properties of both materials, and hence can be superior to either of them in terms of electrical and thermal performance. Compared with Cu-based interconnects, Cu-G interconnects exhibit an enhanced electrical conductivity and current driving capacity [3], [4], a faster data transferring speed [3], a larger thermal conductivity [5], and the resistance to electromigration, therefore a better long-term reliability [6]. However, as far as the modeling of Cu-G interconnect is concerned, most of the existing methods separately model the graphene layers [7], [8] and the hybrid interconnect structure [9]–[12]. Such a decoupled approach may cause accuracy problems in high-frequency simulations for two main reasons. First, as shown in [13], most of these graphene models are no longer sufficient at high frequencies since skin depth becomes comparable to the mean free path. Second, these decoupled electrical conductivity models of graphene [7], [8] assume graphene's steady-state responses to external stimulus. This assumption can be valid for many low-frequency measurements and single-frequency stimuli but is unlikely to hold in emerging high-frequency IC scenarios. The main reason for the failure at high frequencies is the low backscattering frequency (BSF) of graphene (∼100 GHz) [14], [15]. When the signal frequency in Cu-G interconnects becomes high enough to reach the relatively low BSF of graphene, graphene layers may not have enough scatterings to re-equilibrate themselves, thus may not give the physical steady-state response as predicted by steady-state conductivity models. Since the decoupled steady-state models can miss graphene's dynamic electronic responses in high-frequency simulations, a full-wave dynamic modeling and simulation in time domain is needed.

To successfully develop Cu-G new interconnect solutions for high-frequency IC technology, it is necessary to understand the entire physical process that takes place in a Cu-G interconnect. Under a voltage or current source excitation, the electric and magnetic fields are generated in the physical layout of a graphene interconnect. These fields drive the movement of charge carriers in the graphene material. The resultant change in conduction current, in turn, modifies the electric and magnetic field distributions. At high frequencies (e.g., 50 GHz), the graphene layer may not reach a steady state, resulting in a nonlinear conduction current response. To the best of our knowledge, none of the existing models have sufficiently captured the dynamic physics present in the Cu-G interconnects. Hence, they may lose their predictive power when applied to the design of new Cu-G interconnects.

In this article, we develop a multiphysics-based model and an efficient simulation algorithm to cosimulate directly in time-domain Maxwell's equations, equations characterizing

Manuscript received August 1, 2019; revised October 22, 2019; accepted November 10, 2019. Date of publication January 1, 2020; date of current version January 31, 2020. This work was supported by a Grant from the National Science Foundation under Award 1619062. This article is an expanded version from the IEEE MTT-S International Conference on Numerical Electromagnetic and Multiphysics Modeling and Optimization (NEMO2019), Cambridge, MA, USA, May 29-31, 2019. *(Corresponding author: Dan Jiao.)*

The authors are with the School of Electrical and Computer Engineering, Purdue University, West Lafayette, IN 47907 USA (e-mail: djiao@purdue.edu).

Color versions of one or more of the figures in this article are available online at http://ieeexplore.ieee.org.

Digital Object Identifier 10.1109/TMTT.2019.2955123

graphene materials, and the Boltzmann equation from direct current (dc) to high frequencies. To enable the simulation of nanointerconnects within a feasible run time, the entire numerical system is further made unconditionally stable in time marching. In [16], we present a basic idea of this article. In this article, we significantly expand the work in [16]. We detail the multiphysics modeling and simulation algorithm for analyzing Cu-G interconnects, prove the time-domain stability of the coupled simulation, validate the proposed work against measured data, and also apply it to predict the crosstalk and propagation delay of Cu-G interconnects, which has not been reported in open literature.

The rest of this article is organized as follows. In Section II, the proposed multiphysics model of Cu-G hybrid nanointerconnects, including the theories and assumptions, is presented. Section III details an unconditionally stable numerical algorithm to simulate the proposed multiphysics model, followed by a proof to its unconditional stability. Extensive numerical experiments, such as the validation of both Maxwell and Boltzmann solvers, dc conductivity, crosstalk effect, and propagation delay of graphene-encapsulated Cu nanointerconnects, are presented in Section IV. Finally, we summarize this article in Section V.

II. Multiphysics Modeling of Cu-G Hybrid Nanointerconnects

The electromagnetic performance of a Cu-G interconnect is governed by Maxwell's equations from dc to high frequencies

$$\nabla \times \mathbf{E} = -\mu \frac{\partial \mathbf{H}}{\partial t} \tag{1a}$$

$$\nabla \times \mathbf{H} = \epsilon \frac{\partial \mathbf{E}}{\partial t} + \sigma \mathbf{E} + \mathbf{j}_i \tag{1b}$$

where $\mathbf{E}$ is the electric field intensity, $\mathbf{H}$ is the magnetic field intensity, $\mathbf{j}_i$ is the input (supply) current density, and μ, ϵ, and σ are the permeability, permittivity, and conductivity, respectively.

When considering the existence of graphene layers, especially their conduction current density $\mathbf{j}_g = \sigma \mathbf{E}$ in changing the entire electromagnetic response, conventional simplified steady-state σ models [7], [8] can miss the dynamic nonlinear physics at high frequencies, including both the nonlinear buildup of the conduction current in graphene and the nonlinear coupling between the external field and electron behavior inside graphene layers. Therefore, an accurate model requires a direct observation of the charge carriers in graphene, which is described by the distribution function $f(\mathbf{r}, \mathbf{k}, t)$ in phase space (real $\mathbf{r}$-space and momentum $\mathbf{k}$-space). Based on the first principles, $f(\mathbf{r}, \mathbf{k}, t)$ is governed by the following Boltzmann equation:

$$\mathbf{v} \cdot \nabla_{\mathbf{r}} f + \frac{q}{\hbar} \mathbf{E} \cdot \nabla_{\mathbf{k}} f + \frac{\partial f}{\partial t} = -\frac{f - f_0}{\tau} \tag{2}$$

where $\mathbf{v} = d\mathbf{r}/dt$ is the velocity vector, $\mathbf{k} = \mathbf{p}/\hbar$ is the wave vector of Bloch wave in momentum space, q is the amount of charge in each carrier, and $\hbar$ is the Planck constant. The magnetic effects in Boltzmann equation are not considered here as they are much smaller than electric effects in IC interconnects. The scattering term on the right-hand side of the Boltzmann equation is approximated by the relaxation time approximation [17], where τ is the relaxation time, and f_0 is the Fermi-Dirac distribution at the equilibrium state

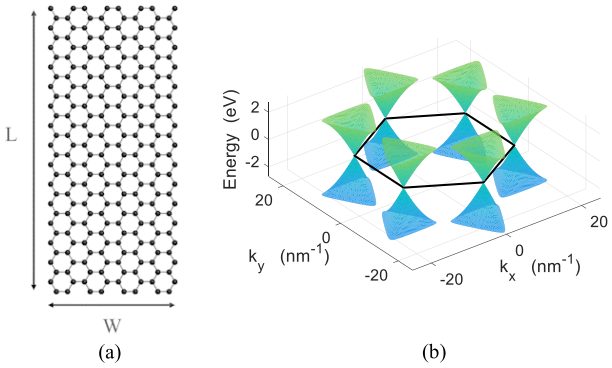

Fig. 1. (a) Structure of a single-layer graphene with length L and width W. (b) Linear dispersion of graphene. Dirac cones are located at the six corners of the hexagonal Brillouin zone. Therefore, the valley degeneracy $g_v = 2$.

$$f_0 = \left[1 + \exp\left(\frac{\xi - \xi_{\mathrm{F}}}{k_{\mathrm{B}} T}\right)\right]^{-1} \tag{3}$$

in which ξ is the carrier's energy, ξ_{F} is the Fermi energy (also called Fermi level or chemical potential), k_{B} is Boltzmann's constant, and T is the temperature.

Given $f(\mathbf{r}, \mathbf{k}, t)$, the conduction current density $\mathbf{j}_g$ in graphene can be evaluated from an integration over $\mathbf{k}$-space as

$$\mathbf{j}_g = \frac{g_s g_v q}{(2\pi)^d} \int_{\mathbf{k}} f \mathbf{v} d\mathbf{k} \tag{4}$$

where g_s and g_v are the spin and valley degeneracy, respectively, and d denotes the problem dimension, which is 2 and 3 in a 2-D and 3-D analyses, respectively. In order to calculate $\mathbf{j}_g$ from (2) and (4), the velocity vector $\mathbf{v}$ needs to be expressed as a function of $\mathbf{k}$. Semiclassically, by treating the Bloch waves as wave packets, the classical velocity $\mathbf{v}$ is defined as the group velocity $d\omega/d\mathbf{k}$ of such wave packets [17]. The frequency ω is associated with a wave function of energy ξ by quantum theory, $\omega = \xi/\hbar$, and hence

$$\mathbf{v} = \nabla_{\mathbf{k}} \xi / \hbar. \tag{5}$$

After substituting the following linear dispersion relation of graphene [18], which is illustrated in Fig. 1(b):

$$\xi = v_{\mathrm{F}} \hbar k \tag{6}$$

where $v_{\mathrm{F}} = 10^6$ m/s is the Fermi velocity and $k = (k_x^2 + k_y^2)^{1/2}$, we can express the velocity vector $\mathbf{v}$ as the following function of $\mathbf{k}$:

$$\mathbf{v}(\mathbf{k}) = \nabla_{\mathbf{k}} \xi / \hbar = v_{\mathrm{F}} \hat{\mathbf{k}} \tag{7}$$

with $\mathbf{k} = k_x \hat{x} + k_y \hat{y}$, and $\hat{\mathbf{k}} = \mathbf{k}/|k|$ being the unit vector along the direction of $\mathbf{k}$.

The proposed system of equations, which governs the electromagnetic performance of Cu-G interconnects, consists of three sets of first-principle equations, namely, Maxwell's equations (1), Boltzmann equation (2), and the dispersion relation of graphene (6). Because the carrier distribution function

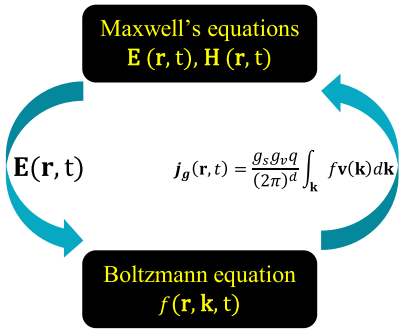

Fig. 2. Illustration of the cosimulation flow.

f is a function of $\mathbf{r}$, $\mathbf{k}$, and t, the computational domain for this model has seven dimensions in 3-D analyses and five dimensions in 2-D analyses. A flow of the cosimulation of these equations in time domain is illustrated in Fig. 2. Given an external source and initial conditions, Maxwell's equations (1) are solved to obtain electric field $\mathbf{E}(\mathbf{r}, t)$, using which the Boltzmann equation (2) can be solved to obtain charge carrier distribution $f(\mathbf{r}, \mathbf{k}, t)$. From integrating $f(\mathbf{r}, \mathbf{k}, t)$ over $\mathbf{k}$-space as shown in (4), the conduction current density $\mathbf{j}_g(\mathbf{r}, t)$ in graphene layers is calculated at each space point. At the next time instant, graphene's conduction current density term $\sigma\mathbf{E}$ in Maxwell's equations (1) is replaced by latest $\mathbf{j}_g(\mathbf{r}, t)$, while the conduction current density in other conducting materials is still updated using $\sigma\mathbf{E}$. Now, with all the current updated, Maxwell's equations (1) are ready to be solved again. The whole process continues until a desired time is reached or until the physical phenomenon happening in a Cu-G interconnect has reached its steady state.

III. Multiphysics Cosimulation in Time Domain and Stability Analysis

There are two major challenges in the multiphysics simulation of Cu-G interconnects. The first challenge is that Boltzmann equation (2) is a 7-D equation in a 3-D analysis, which is computationally expensive. To reduce the computational cost, we utilize the fact that graphene is a 2-D material, hence we can solve a 2-D version of Boltzmann equation (2) in conjunction with the 3-D Maxwell's equations. However, even using a 2-D Boltzmann equation, there are five dimensions involved, making the simulation of Boltzmann subsystem much slower than that of the Maxwell subsystem. The second challenge arises from the small size of nanointerconnects, which results in a large number of time steps to finish one simulation using explicit solvers. To address this problem, we develop an unconditionally stable cosimulation algorithm to remove the dependence of time step on space step.

A. Unconditionally Stable Time-Marching Scheme of the Maxwell Subsystem

In this article, we apply an implicit unconditionally stable time-domain scheme developed in [19] to a finite-difference time-domain (FDTD)-based discretization of Maxwell's equations. This scheme is theoretically proved to be unconditionally stable for general problem settings having arbitrary structures and inhomogeneous materials. In this method, we discretize Maxwell's equations (1) as

$$\mathbf{S}_e\{e\}^{n+1} = -\mathbf{D}_\mu \frac{\{h\}^{n+\frac{1}{2}} - \{h\}^{n-\frac{1}{2}}}{\Delta t} \tag{8a}$$

$$\mathbf{S}_h\{h\}^{n+\frac{1}{2}} = \mathbf{D}_\epsilon \frac{\{e\}^{n+1} - \{e\}^n}{\Delta t} + \mathbf{D}_\sigma\{e\}^{n+1} + \{j_g\}^n + \{j_i\}^{n+1} \tag{8b}$$

where $\{e\}^n$ represents the vector of electric field intensities at the nth time instant, $\{h\}^{n+(\frac{1}{2})}$ represents the vector of magnetic field intensities at the $n + (\frac{1}{2})$ time instant, $\{j_g\}$ represents the vector of conduction current densities in graphene layers, $\{j_i\}$ represents the input current densities, and $\mathbf{D}_\mu$, $\mathbf{D}_\epsilon$, and $\mathbf{D}_\sigma$ are diagonal matrices of permeability, permittivity, and conductivity, respectively. The matrix-vector products $\mathbf{S}_e\{e\}$ and $\mathbf{S}_h\{h\}$ represent discretized $\nabla \times \mathbf{E}$ and $\nabla \times \mathbf{H}$. The $\mathbf{S}_e$ and $\mathbf{S}_h$ can be readily constructed using a single-grid patch based FDTD formulation developed in [20].

If we eliminate $\{h\}$ in (8), we will end up with the following backward-difference-based discretization of the second-order vector wave equation for $\mathbf{E}$ if $\{j_g\}$ is not considered:

$$\{e\}^{n+1} - 2\{e\}^n + \{e\}^{n-1} + \Delta t\mathbf{D}_\epsilon^{-1}\mathbf{D}_\sigma(\{e\}^{n+1} - \{e\}^n) + \Delta t^2\mathbf{D}_\epsilon^{-1}\mathbf{S}_h\mathbf{D}_\mu^{-1}\mathbf{S}_e\{e\}^{n+1} = -\Delta t^2\mathbf{D}_\epsilon^{-1}\left(\frac{\partial\{j\}}{\partial t}\right)^{n+1}. \tag{9}$$

Discarding the source term since it has nothing to do with the stability, and performing a z-transform of the above time-marching equation, we can find

$$|z| = \frac{1}{\sqrt{1 + \Delta t^2\lambda}}, \tag{10}$$

where λ is the eigenvalue of $\mathbf{D}_\epsilon^{-1}\mathbf{S}_h\mathbf{D}_\mu^{-1}\mathbf{S}_e$. Since in an FDTD method, $\mathbf{S}_h = \mathbf{S}_e^T$ is satisfied in a uniform grid [20], the eigenvalues of $\mathbf{D}_\epsilon^{-1}\mathbf{S}_h\mathbf{D}_\mu^{-1}\mathbf{S}_e$ are always nonnegative. Substituting $\lambda \geq 0$ into (10), it can be readily found that z's modulus is always bounded by 1 regardless of Δt. Hence, the time marching of (9) is ensured to be unconditionally stable. Although it appears that we have to solve a matrix in the time marching, using the scheme developed in [19], this matrix's inverse can be explicitly found, thus avoiding a matrix solution.

The updating from one time step to the next in (8) can also be rewritten as

$$\mathbf{M}_A\{x\}^{n+1} = \mathbf{M}_B\{x\}^n + \{b_j\}^{n+1} \tag{11}$$

where

$$\{x\}^n = \begin{bmatrix} \{e\}^n \\ \{h\}^{n-\frac{1}{2}} \end{bmatrix} \text{ and } \{b_j\}^{n+1} = \begin{bmatrix} -\{j_g\}^n - \{j_i\}^{n+1} \\ 0 \end{bmatrix}$$

and

$$\mathbf{M}_A = \begin{bmatrix} \frac{\mathbf{D}_\epsilon}{\Delta t} + \mathbf{D}_\sigma & -\mathbf{S}_h \\ \mathbf{S}_e & \frac{\mathbf{D}_\mu}{\Delta t} \end{bmatrix} \text{ and } \mathbf{M}_B = \begin{bmatrix} \frac{\mathbf{D}_\epsilon}{\Delta t} & 0 \\ 0 & \frac{\mathbf{D}_\mu}{\Delta t} \end{bmatrix}.$$

B. Unconditionally Stable Time-Marching Scheme of the Boltzmann Subsystem

The high dimensionality of the phase space makes solving the Boltzmann equation (2) a challenging task. One of the biggest obstacles for a deterministic Boltzmann solver is the requirement of huge memory. To resolve the memory issue, the past few decades have seen many efforts along two major directions for solving the Boltzmann equation. One direction is the Monte Carlo approach, where the Boltzmann equation is solved by simulating a stochastic process [21]–[23]. Another direction is to expand the distribution function f with basis functions in $\mathbf{k}$-space, and then truncate the expansion to the first few terms according to the accuracy. The commonly used expansions are spherical harmonics expansion [24] and Fourier harmonics expansion in quantized $\mathbf{k}$-space [25]. Both of the two directions can reduce the required memory by a few orders. However, the disadvantages are: 1) the simplification of the original Boltzmann equation and 2) the requirement of a self-iterative solver to determine a few key parameters like the expansion coefficient. These existing Boltzmann solvers can hardly provide the dynamic time-domain nonlinear transition we want to capture from the original Boltzmann equation (2). Therefore, in this article, we develop a direct deterministic Boltzmann solver for the Cu-G system. The advancement of dynamic random access memory (DRAM) technology and today's computers has greatly alleviated the limitation from huge memory requirements. On the other hand, the 2-D nature of graphene reduces the dimension of phase space from six to four. These two factors make a direct deterministic Boltzmann solver feasible for the Cu-G hybrid nanointerconnects.

However, the direct Boltzmann solver still needs to be carefully developed to resolve two challenges. First, the extremely small space step could require an extremely small time step due to the stability requirement. For example, in one Cu-G hybrid nanointerconnect to be shown later, a conditionally stable Boltzmann solver can require millions of time steps to finish one run. Because of the expensive computational cost for the Boltzmann subsystem, the need for simulating many time steps can significantly degrade the efficiency of the simulation. Second, the coupling with the Maxwell subsystem should not ruin the stability, or should even maintain the global unconditional stability of the entire system. Both of the challenges are solved with the following unconditionally stable Boltzmann solver.

1) Unconditionally Stable Boltzmann Solver: Substituting (7) into (2), the 2-D Boltzmann equation for graphene in the 4-D phase space $(x-y-k_x-k_y)$ becomes

$$\frac{v_{\mathrm{F}}}{k}\left(k_x\frac{\partial f}{\partial x}+k_y\frac{\partial f}{\partial y}\right)+\frac{q}{\hbar}\left(E_x\frac{\partial f}{\partial k_x}+E_y\frac{\partial f}{\partial k_y}\right)+\frac{\partial f}{\partial t}=-\frac{f-f_0}{\tau}. \tag{12}$$

In terms of the discretization of the derivatives, the independence among $\mathbf{r}$, $\mathbf{k}$, and t allows us to consider each first-order derivative independently. First, $\nabla_{\mathbf{r}}$ is discretized with a central difference to maintain the same accuracy $\sim\mathcal{O}(\Delta r^2)$ as that in FDTD. Second, $\nabla_{\mathbf{k}}$ is also discretized with a central difference to align with the $\nabla_{\mathbf{r}}$. Mathematically, the role of $\mathbf{r}$ and $\mathbf{k}$ in the Boltzmann equation (12) can be exchanged without changing the equation much. Thus, aligning the numerical treatment of $\mathbf{r}$ and $\mathbf{k}$ can simplify the system matrices and thereby the solution of the Boltzmann subsystem. Having $\nabla_{\mathbf{r}}$ and $\nabla_{\mathbf{k}}$ discretized with the central difference in phase space, the remaining $\partial/\partial t$ could be discretized in time with a backward difference to guarantee the unconditional stability. As a result, we obtain

$$\left(\mathbf{S}_r+\mathbf{S}_k^n\right)\{f\}^{n+1}+\frac{\{f\}^{n+1}-\{f\}^n}{\Delta t}=\frac{\{f_0\}-\{f\}^{n+1}}{\tau} \tag{13}$$

where $\{f\}^n$ is the vector of carrier distribution function at the nth time instant, and $\mathbf{S}_r\{f\}$ and $\mathbf{S}_k^n\{f\}$ represent discretized $\mathbf{v}\cdot\nabla_{\mathbf{r}}f$ and $(q/\hbar)\mathbf{E}\cdot\nabla_{\mathbf{k}}f$, respectively. Here, the superscript n of $\mathbf{S}_k^n$ denotes the time instant of $\mathbf{E}$ used to obtain $\mathbf{S}_k^n$. The grid used for discretizing Maxwell's equations is also used for solving the Boltzmann subsystem, and the f is assigned at the $\mathbf{H}$'s points. The electric field $\mathbf{E}$ used in the Boltzmann equation is center-averaged by neighboring $\mathbf{E}$ fields in the grid. The matrix-based expression here follows a similar logic as that in the Maxwell subsystem. All local $f(i,j,i_k,j_k)$ in the 4-D phase space are reorganized and labeled with a global index

$$m_{i,j}^{i_k,j_k}=j_kN_xN_yN_{k_x}+i_kN_xN_y+jN_x+i \tag{14}$$

in which N_x, N_y, and N_{k_x} are the number of nodes along the x-, y-, and k_x-directions, respectively. The local index (i,j,i_k,j_k) means the position in phase space is at $(x=i\Delta x+x_0, y=j\Delta y+y_0, k_x=i_k\Delta k_x+k_{x0}, k_y=j_k\Delta k_y+k_{y0})$, where $(\Delta x,\Delta y,\Delta k_x,\Delta k_y)$ and (x_0,y_0,k_{x0},k_{y0}) denote the cell size, and starting point along each dimension. Thus, each local $f(i,j,i_k,j_k)$ becomes the $m_{i,j}^{i_k,j_k}$th element $f_{m_{i,j}^{i_k,j_k}}$ in vector $\{f\}$.

The entries of two matrices $\mathbf{S}_r$ and $\mathbf{S}_k^n$, using a central difference in a uniform grid, can be analytically extracted as the following. Take $\mathbf{S}_r\{f\}\sim\mathbf{v}\cdot\nabla_{\mathbf{r}}f$ as an example. Since in $\mathbf{v}\cdot\nabla_{\mathbf{r}}f$, we use nearby f values to generate a value $\tilde{f}$ at a local point (i,j,i_k,j_k), the central-difference formula written in local indices is

$$\begin{aligned}\tilde{f}(i,j,i_k,j_k)&=v_x(i_k,j_k)\frac{f(i+1,j,i_k,j_k)-f(i-1,j,i_k,j_k)}{2\Delta x}\\&\quad+v_y(i_k,j_k)\frac{f(i,j+1,i_k,j_k)-f(i,j-1,i_k,j_k)}{2\Delta y}.\end{aligned}$$

This formula, if written in global indices (14), becomes

$$\tilde{f}_{m_{i,j}^{i_k,j_k}}=v_{x\,m_{0,0}^{i_k,j_k}}\frac{f_{m_{i+1,j}^{i_k,j_k}}-f_{m_{i-1,j}^{i_k,j_k}}}{2\Delta x}+v_{y\,m_{0,0}^{i_k,j_k}}\frac{f_{m_{i,j+1}^{i_k,j_k}}-f_{m_{i,j-1}^{i_k,j_k}}}{2\Delta y} \tag{15}$$

which is simply a row of the matrix-based expression $\{\tilde{f}\}=\mathbf{S}_r\{f\}\sim\mathbf{v}\cdot\nabla_{\mathbf{r}}f$. Since $\mathbf{v}$ is independent of $\mathbf{r}$ for graphene here, the (i,j) indices for $\mathbf{v}$ are denoted as $(0,0)$. The elements of matrix $\mathbf{S}_r$, hence, can be directly extracted from (15) as

$$\begin{aligned}\mathbf{S}_{r\,m_{i,j}^{i_k,j_k},m_{i+1,j}^{i_k,j_k}}&=v_{x\,m_{0,0}^{i_k,j_k}}/(2\Delta x)=-\mathbf{S}_{r\,m_{i,j}^{i_k,j_k},m_{i-1,j}^{i_k,j_k}}\\\mathbf{S}_{r\,m_{i,j}^{i_k,j_k},m_{i,j+1}^{i_k,j_k}}&=v_{y\,m_{0,0}^{i_k,j_k}}/(2\Delta y)=-\mathbf{S}_{r\,m_{i,j}^{i_k,j_k},m_{i,j-1}^{i_k,j_k}}.\end{aligned} \tag{16}$$

For the other matrix $\mathbf{S}_k^n\{f\} \sim \frac{q}{\hbar}\mathbf{E}\cdot\nabla_{\mathbf{k}} f$, we can find its elements similarly by exchanging $\mathbf{E}$ to $\mathbf{v}$ and $\mathbf{k}$ to $\mathbf{r}$.

The proposed time-marching formula for the Boltzmann subsystem (13) is

$$\mathbf{B}^n\{f\}^{n+1} = \{f\}^n + \{\tilde{f_0}\} \tag{17}$$

where the constant term $\{\tilde{f_0}\} = \{f_0\}\Delta t/\tau$ and the system matrix

$$\mathbf{B}^n = (1 + \Delta t/\tau)\mathbf{I} + \Delta t\big(\mathbf{S}_r + \mathbf{S}_k^n\big). \tag{18}$$

2) Proof on the Unconditional Stability of the Boltzmann Solver and the Choice of Time Step: To analyze the stability, the eigenvalues of matrix $\mathbf{B}^n$, thereby the eigenvalues of $\mathbf{S}_r$ and $\mathbf{S}_k^n$, should be studied. Here, we first prove that both $\mathbf{S}_r$ and $\mathbf{S}_k^n$, with a central difference in a uniform grid, are skew-symmetric. Still take $\mathbf{S}_r\{f\} \sim \mathbf{v}\cdot\nabla_{\mathbf{r}} f$ as an example. From the matrix elements in (16), the transpose of matrix element $\mathbf{S}_{r\,m_{i,j}^{i_k,j_k},m_{i+1,j}^{i_k,j_k}}$ is $\mathbf{S}_{r\,m_{i+1,j}^{i_k,j_k},m_{i,j}^{i_k,j_k}}$, whose value is the opposite of $\mathbf{S}_{r\,m_{i,j}^{i_k,j_k},m_{i+1,j}^{i_k,j_k}}$. The same procedure can be applied to j. Thus, the skew-symmetry of $\mathbf{S}_r$ is proved. The key factors to the skew-symmetry are: 1) the velocity $\mathbf{v}$ is independent of $\mathbf{r}$-space and 2) the $\mathbf{r}$-space is discretized uniformly along each direction. These two together guarantee the matrix elements in (16) to be the same, regardless of the choice of (i, j). For the other matrix $\mathbf{S}_k^n\{f\} \sim (q/\hbar)\mathbf{E}\cdot\nabla_{\mathbf{k}} f$, we can exchange $\mathbf{E}$ to $\mathbf{v}$ and $\mathbf{k}$ to $\mathbf{r}$ and end up with a similar proof.

As a result of skew-symmetry, the eigenvalues of $\mathbf{S}_r + \mathbf{S}_k^n$ are purely imaginary [26]. From the expression of matrix $\mathbf{B}^n$ in (18), we can see clearly that its eigenvalues are

$$\lambda(\mathbf{B}^n) = 1 + \Delta t/\tau + \Delta t\lambda\big(\mathbf{S}_r + \mathbf{S}_k^n\big).$$

Since $\lambda(\mathbf{S}_r + \mathbf{S}_k^n)$ are purely imaginary, we have

$$|\lambda(\mathbf{B}^n)| = \sqrt{(1 + \Delta t/\tau)^2 + \Delta t^2|\lambda\big(\mathbf{S}_r + \mathbf{S}_k^n\big)|^2} \geq 1. \tag{19}$$

Hence, the amplification factor of Boltzmann subsystem $\mathbf{B}^n\{f\}^{n+1} = \{f\}^n$ is bounded by 1, regardless of the choice of time step. As a result, we prove the proposed time marching of Boltzmann subsystem is unconditionally stable.

The unconditional stability allows for a choice of any large time step without affecting stability. Hence, in real simulations, the time step can be solely chosen according to the accuracy requirement. The relaxation time approximation in Boltzmann equation (2) assumes an exponential decay with a relaxation time τ. Therefore, the physical process gives the Boltzmann subsystem a characteristic time constant τ. According to the sampling theorem, an accurate time step to capture the time constant τ in the Boltzmann subsystem would be

$$\Delta t \leq \tau/10. \tag{20}$$

C. Unconditionally Stable Time-Marching Scheme of the Coupled System

As for the coupling between the Maxwell subsystem and the Boltzmann subsystem, the Boltzmann subsystem directly uses the electric field intensity $\mathbf{E}$ from the Maxwell subsystem, whereas the Maxwell subsystem uses, indirectly from the Boltzmann subsystem, the conduction current density $\{j_g\}^n$ in graphene layers. The $\{j_g\}^n$ is evaluated from $\{f\}^n$ through the integration of (4), which is numerically evaluated from a trapezoidal integration rule to maintain the second-order accuracy in the truncated $\mathbf{k}$-space. For a surface conduction current density, the x-component of (4) can be written as

$$j_{gx\_2D}^n = \frac{g_s g_v q}{(2\pi)^2}\int_{k_x}\int_{k_y} f^n v_x dk_x dk_y \tag{21}$$

a 2-D trapezoidal integration of which yields

$$j_{gx\_2D}^n(i, j) = \frac{g_s g_v q}{(2\pi)^2}\frac{\Delta k_x \Delta k_y}{4}\sum_{i_k=0}^{N_{k_x}-1}\sum_{j_k=0}^{N_{k_y}-1}\alpha(i_k, j_k) f^n(i, j, i_k, j_k) v_x(i_k, j_k) \tag{22}$$

where the coefficient $\alpha(i_k, j_k) = 4$ inside the k_x-k_y grid, $\alpha(i_k, j_k) = 2$ on the four outermost boundaries of the grid, and $\alpha(i_k, j_k) = 1$ at four corners of the grid. The y-component of $j_{g\_2D}^n$ can be obtained by changing v_x in (22) to v_y. After replacing the local index of $f^n(i, j, i_k, j_k)$ with global index (14), the numerical trapezoidal integration (22) could be expressed by a matrix-vector product of $\{j_g\}_{2D}^n = \mathbf{S}_{j\_2D}\{f\}^n$. The $\{j_g\}_{2D}^n$ here is a surface current density, which agrees with the fact that graphene is a 2-D material whose current flow is a sheet current flow. However, Maxwell's equations require a volume current density $\{j_g\}^n$. Here, we can treat a graphene layer as a thin sheet [11] and obtain an equivalent volume current density $\{j_g\}^n = \{j_g\}_{2D}^n/dz$ [27], where dz is the grid size perpendicular to the graphene sheet. Thus, by using $\mathbf{S}_j = \mathbf{S}_{j\_2D}/dz$, we obtain

$$\{j_g\}^n = \mathbf{S}_j\{f\}^n. \tag{23}$$

The coupled systems of equations, including the Maxwell subsystem (11), the Boltzmann subsystem (17), and the coupling mechanism through conduction current density (23), constitute a nonlinear system of equations, as shown in the following:

$$\begin{bmatrix}\mathbf{M}_A & 0\\ 0 & \mathbf{B}^n\end{bmatrix}\begin{bmatrix}\{x\}^{n+1}\\ \{f\}^{n+1}\end{bmatrix} = \begin{bmatrix}\mathbf{M}_B & \mathbf{M}_j\\ 0 & \mathbf{I}\end{bmatrix}\begin{bmatrix}\{x\}^n\\ \{f\}^n\end{bmatrix} + \begin{bmatrix}\{x_0\}^{n+1}\\ \{\tilde{f_0}\}\end{bmatrix} \tag{24}$$

where

$$\mathbf{M}_j = \begin{bmatrix}-\mathbf{S}_j\\ 0\end{bmatrix} \text{ and } \{x_0\}^{n+1} = \begin{bmatrix}-\{j_i\}^{n+1}\\ 0\end{bmatrix}.$$

Given an initial condition $\{x\}^0$ and $\{f\}^0$, and the excitation $\{x_0\}$, we can update the system in time based on (24), and finally obtain the full-wave response of general 3-D Cu-G hybrid nanointerconnects.

Next, we prove that the proposed time marching of the cosimulation system shown in (24) is unconditionally stable. Since the constant terms and excitation are irrelevant to stability, they are ignored in the following stability analysis. For the coupled nonlinear system of equations (24), at every time step, we have

$$\begin{bmatrix}\{x\}^{n+1}\\ \{f\}^{n+1}\end{bmatrix} = \begin{bmatrix}\mathbf{M}_A^{-1}\mathbf{M}_B & \mathbf{M}_A^{-1}\mathbf{M}_j\\ 0 & (\mathbf{B}^n)^{-1}\end{bmatrix}\begin{bmatrix}\{x\}^n\\ \{f\}^n\end{bmatrix} = \mathbf{G}^n\begin{bmatrix}\{x\}^n\\ \{f\}^n\end{bmatrix}. \tag{25}$$

As can be seen, the amplification matrix $\mathbf{G}^n$ is a block upper triangular matrix, whose eigenvalues $\{\lambda(\mathbf{G}^n)\}$ consist of the eigenvalues of the two diagonal block matrices $\mathbf{M}_A^{-1}\mathbf{M}_B$, and $(\mathbf{B}^n)^{-1}$, namely

$$\{\lambda(\mathbf{G}^n)\} = \left\{\lambda\left(\mathbf{M}_A^{-1}\mathbf{M}_B\right)\right\} \oplus \{\lambda((\mathbf{B}^n)^{-1})\}.$$

In other words, the overall stability of the coupled nonlinear system (24) is decoupled and determined by the stability of each subsystem (11) and (17). Because both $|\lambda(\mathbf{M}_A^{-1}\mathbf{M}_B)|$ and $|\lambda((\mathbf{B}^n)^{-1})|$ are bounded by 1, all the $|\lambda(\mathbf{G}^n)|$, thereby $\rho(\mathbf{G}^n)$ are bounded by 1; hence, we prove that the cosimulation algorithm (24) is unconditionally stable for an arbitrary choice of time step. Note that, in this cosimulation scheme (24), neither of the two physical coupling flows determines the overall time marching stability. The first coupling flow from the Maxwell part, manifested by the electric field $\mathbf{E}$ in Boltzmann subsystem, enters system matrix $\mathbf{S}_k^n$ but cannot change its skew-symmetry, thus cannot determine the stability of the Boltzmann subsystem. The second coupling flow from the Boltzmann part, the conduction current density of graphene, becomes the off-diagonal block in (24), thus cannot determine the eigenvalues thereby the stability of the Maxwell subsystem.

The unconditional stability of the entire system allows both Maxwell and Boltzmann subsystems to use the same arbitrary time step, despite their different characteristic time constants. Hence, the time step can be chosen solely based on accuracy. For the Boltzmann subsystem, the sampling theorem sets an upper limit of the accurate time step. The characteristic time constant of the Maxwell subsystem is usually determined by the main signal frequency ν_{sig}, which requires a $\Delta t \leq 1/(10\nu_{\text{sig}})$. Taking into account Boltzmann's time step requirement (20), an accurate time step for the entire coupled system would be

$$\Delta t \leq \min\{\tau/10, 1/(10\nu_{\text{sig}})\}. \tag{26}$$

Since both Maxwell and Boltzmann subsystems use backward difference in time, the overall accuracy in time for each subsystem as well as for the whole coupled system is $\mathcal{O}(\Delta t)$, while the accuracy in space is of second order.

IV. Numerical Results

In this section, we first validate the accuracy of the proposed multiphysics solvers by comparing our numerical results with measurements. After validating both Maxwell and Boltzmann solvers, we proceed to simulate realistic graphene-encapsulated Cu nanointerconnects [3] and analyze their dc conductivity, crosstalk effect, and propagation delay.

A. Validation of the Maxwell Solver

We first validate the accuracy of the proposed work by simulating a realistic test-chip interconnect structure, which is fabricated using a silicon processing technology [28]. This 100-μm-long test-chip interconnect comprises three metal layers and five inhomogeneous dielectric stacks, whose cross-sectional view is illustrated in Fig. 3. Fig. 3 also shows all geometrical dimensions and the relative permittivity ϵ_r of each layer. A current source of a time-derivative Gaussian

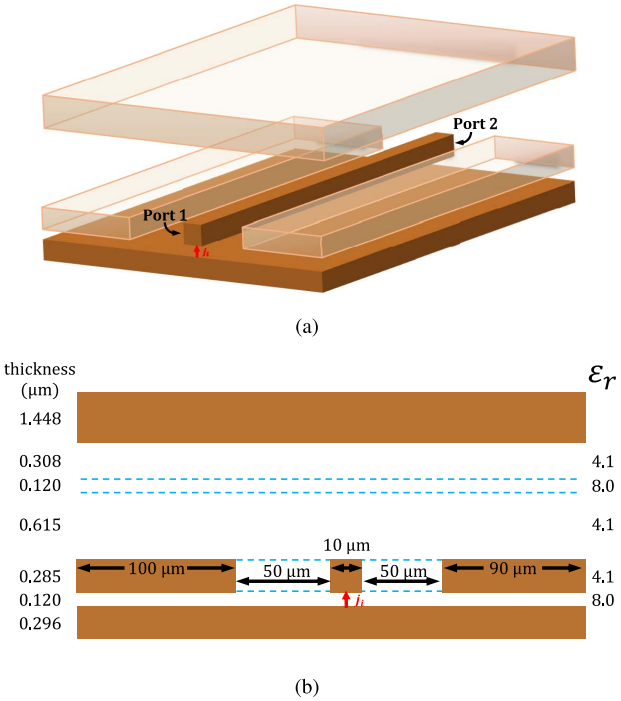

Fig. 3. Geometry of a test-chip interconnect. (a) 3-D view of three metal layers, where the current source is supplied from bottom metal layer to the center wire at port 1. (b) Front view of the test-chip interconnect.

pulse $j_i = -(t - t_0)\exp[-((t - t_0)/\tau_s)^2]$ A/m^2 ($t_0 = 4\tau_s$, $\tau_s = 2 \times 10^{-11}$ s) is placed right in the middle at the near-end of the center interconnect. The 100-μm-long interconnect is sandwiched between two 20-μm-long air layers in the front and at the back. The smallest mesh size used in the simulation is 0.04 μm, and the time step for time marching is 4×10^{-13} s due to the proposed unconditionally stable method. After performing a fast Fourier transform (FFT) on the current source and the simulated time-domain port voltages, we directly obtain the Z-parameters of the structure, which are then converted into S-parameters with a 50-Ω reference impedance. The S-parameters of this test-chip interconnect are measured in the frequency range of 45 MHz–40 GHz using an HP8510 system, where the undesirable signals from cables and probes are further removed following the short-open-load-thru (SOLT) technique, meanwhile the remaining noises generated by the bondpads, vias, and access lines are deembedded using a YZ-matrix technique [28]. The simulated S-parameters and measured ones, as shown in Fig. 4, agree very well with each other.

B. Validation of the Boltzmann Solver

When numerically solving Boltzmann equation (2) for nanometer-scale structures, we choose the backward difference method (13) because of its unconditional stability as proved in Section III. The other common difference methods for discretizing a first-order time derivative equation (2) are either unstable (e.g., central difference method) or conditionally stable (e.g., forward difference method and Crank–Nicholson method). Fig. 5(a) shows that the backward difference method (13) allows for the use of a large time

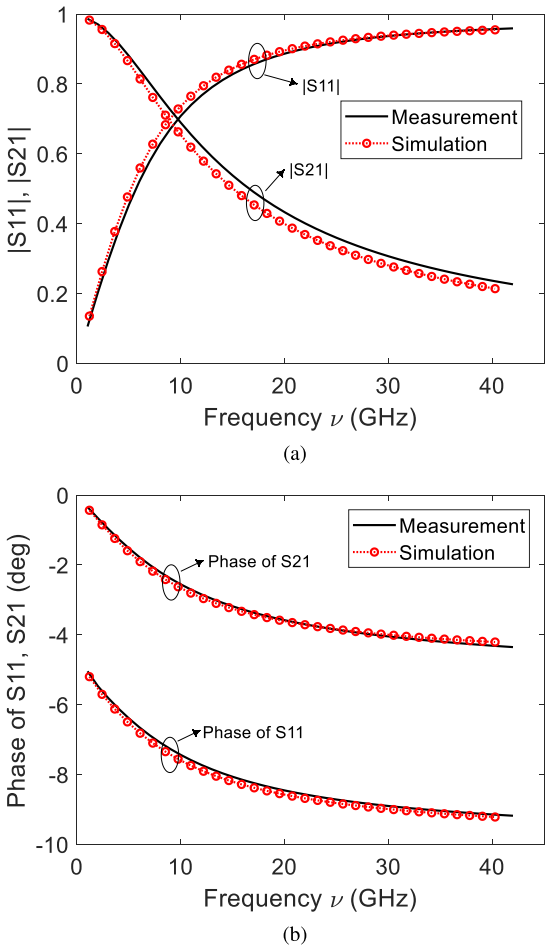

Fig. 4. Simulated S-parameters of a test-chip interconnect in comparison with measurements. (a) Magnitude of S_{11} and S_{21}. (b) Phase of S_{11} and S_{21}.

step irrespective of the extremely small space step. In this example, initial f is Fermi-Dirac distribution (3), Fermi energy $\xi_F = 0.21$ eV, relaxation time $\tau = 4 \times 10^{-11}$ s, the electric field $E_y = 2 \times 10^4$ V/m, $dx = 0.018$ μm, and $dy = 0.5$ μm. All three methods use the same $dt = 2 \times 10^{-11}$ s. After performing the time marching for a long time, only backward difference method remains stable. When approaching the steady state, the backward difference method also exhibits a much smaller unphysical oscillation caused by numerical error.

As for the accuracy, we find all three methods, backward, forward, and Crank–Nicholson methods, give similar results as long as the time step dt is accurately chosen based on the sampling theorem. Taking Boltzmann equation (2) as an example, the characteristic time length is the relaxation time τ, thus a time step $dt = \tau/20$ would be an accurate choice. Within the interval of such a time step, the time dependence of physical quantities does not go beyond linear, and therefore, backward, forward, and central differences should produce the same result in terms of approximating the time derivative. To further investigate the convergence rate, a new example is specifically designed and illustrated in Fig. 5(b). To make all three methods stable when using the same time step $dt = \tau/20$, we adopt a large grid $dx = 5.4$ μm and $dy = 5$ μm, and a smaller electric field $E_y = 2 \times 10^3$ V/m. The other

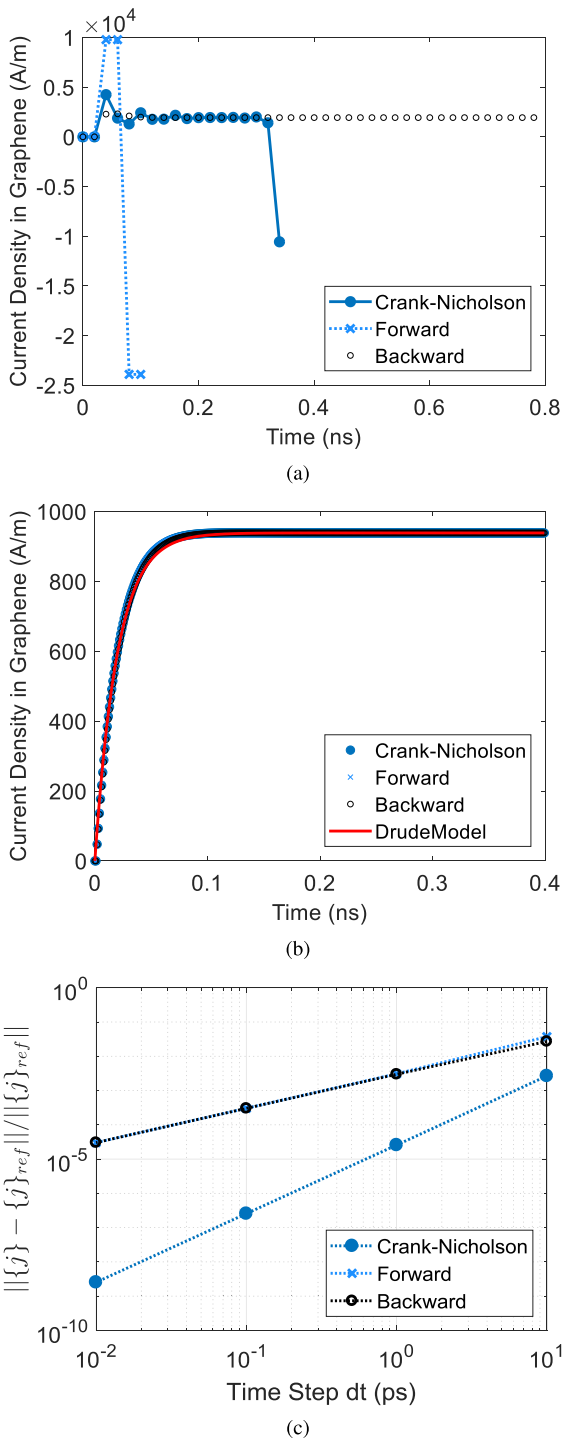

Fig. 5. Surface current density in a graphene layer under a constant electric field E_y. (a) Extremely small grid and large electric field: $dx = 0.018$ μm, $dy = 0.5$ μm, and $E_y = 2 \times 10^4$ V/m. The $dt = 2 \times 10^{-11}$ s. (b) Larger grid and smaller electric field: $dx = 5.4$ μm, $dy = 5$ μm, and $E_y = 2 \times 10^3$ V/m. The $dt = 1 \times 10^{-12}$ s. (c) Error as a function of time step.

parameters remain the same as shown in Fig. 5(a). The current density solved from the backward difference method, as shown in Fig. 5(b), agrees very well with those from other methods, including the Drude model. In Fig. 5(c), we plot the error as a function of time step, where the error is assessed by $\|\{j\}-\{j_{ref}\}\|/\|\{j_{ref}\}\|$, in which the Crank–Nicholson method with $dt = 1 \times 10^{-15}$ s is employed as the reference

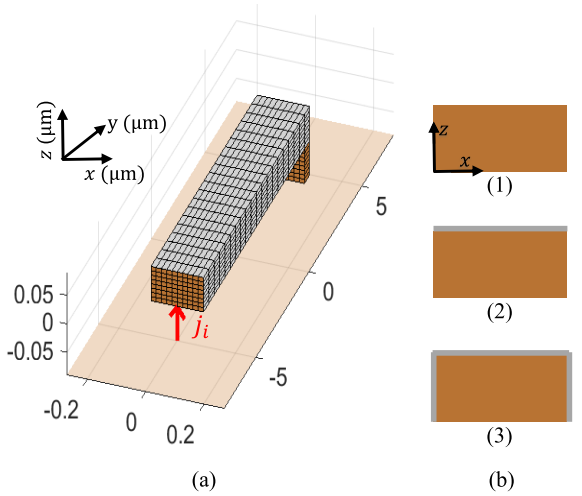

Fig. 6. (a) Geometry and discretization of a Cu-G nanowire whose far-end is shorted to the ground PEC. The graphene layers, in gray color, are coated on top, left, and right surfaces. (b) Front view of the near-end. (1) Bare Cu without graphene coating. (2) Single graphene layer coated on the top surface. (3) Corresponds to the structure in (a).

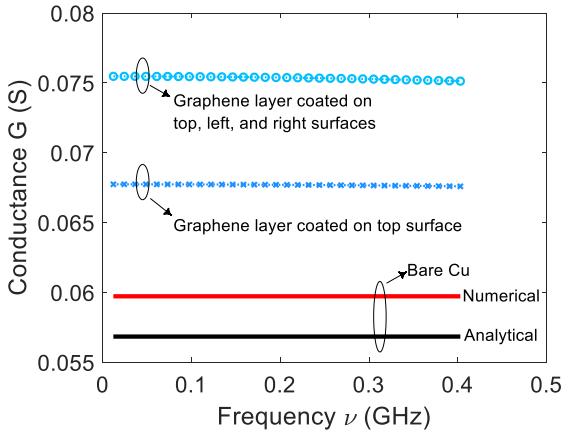

Fig. 7. Simulated conductance G of the three interconnect structures in Fig. 6.

solution $\{j_{ref}\}$, and norm-2 is used. The $\{j\}$ is from either the backward or the forward difference, which includes j at all of the simulated time instants. As can be seen, the backward difference can produce accurate results, and its convergence rate is of first order as theoretically expected.

Another feasible validation is the surface dc conductivity $\sigma_{\text{dc\_2d}}$ of a graphene sheet. Although the model developed in this article aims at the high-frequency and nonlinear responses of graphene, the solver can also accurately reproduce the measured $\sigma_{\text{dc\_2d}}$. One measurement, using the well-known four-point measurements by injecting an excitation current through graphene ribbon and measuring the voltage drop, reports a $\sigma_{\text{dc\_2d}} = 0.015$ S [14] for a graphene sheet of Fermi energy $\xi_{\text{F}} = 0.21$ eV, mean free path $l = 600$ nm, and therefore, relaxation time $\tau = l/v_{\text{F}} = 6 \times 10^{-13}$ s. After substituting these parameters into the simulations as shown in Fig. 5, and dividing the steady-state surface current density j_y by the constant electric field E_y, the proposed Boltzmann solver gives a simulated $\sigma_{\text{dc\_2d}} = 0.0147$ S, which agrees very well with the measurements since the relative error is only 2.0%.

C. Enhanced Electrical Conduction in Cu-G Nanowires Predicted by the Coupled Solver for Multiphysics Simulation

With both the Maxwell solver and the Boltzmann solver validated, next, we employ the proposed coupled Maxwell–Boltzmann solver to simulate a Cu nanowire encapsulated by a single graphene layer on the top, left, and right sides, as illustrated in Fig. 6. The size of the Cu stripline, $W = 180$ nm, $H = 60$ nm, and $L = 10$ μm, is similar to that of a measured Cu-G nanowire [3], whose conductance is measured with standard four-point techniques. We use a uniform regular grid to discretize the Cu into $10 \times 8 \times 20$ grid cells. Graphene layers have a relaxation time $\tau = 2 \times 10^{-11}$ s and a Fermi energy $\xi_{\text{F}} = 0.21$ eV, based on which we truncate the effective **k**-space into an energy range from 0 to $2\xi_{\text{F}}$. Then, we discretize the truncated 2-D **k**-space with 10×20 grid cells. The Maxwell computation domain is a box with perfect electric conductor (PEC) boundaries at the top and the bottom, and perfect magnetic conductor (PMC) boundaries at the other four sides. To see the full-wave response of such a Cu-G nanowire, we inject into the structure a current source whose waveform is a Gaussian derivative in time, $j_i = -10^{16}(t - t_0)\exp[-((t - t_0)/\tau_s)^2]$ A/m^2, where $t_0 = 4\tau_s$ and $\tau_s = 2 \times 10^{-9}$ s, indicating a maximal signal frequency of approximately 0.5 GHz. For the aforementioned real-space grid, conventional FDTD requires a small Δt, therefore, about 10^8 time steps to finish the simulation in the width of a full pulse. However, in our unconditionally stable algorithm (24), only 200 time steps are simulated, where time step is solely determined by the accuracy requirement.

We perform a Fourier transform of the time-domain data and calculate the admittance $Y(\omega) = I_{\text{input}}(\omega)/V_{\text{drop}}(\omega)$, whose real part, the conductance G, is plotted in Fig. 7. The numerical and analytical conductance G of the bare Cu case, plotted in solid lines in Fig. 7, shows a fairly good correlation with an error of 5.07%. Compared with the numerical G in bare Cu structure, a single graphene layer's coating on the top surface enhances the conductance G by 13.4%, whereas the coating on three sides enhances G by 26.4%. For the structure in Fig. 6(a), measurement [3] reports a 22% enhancement on G, which is very close to the simulated 26.4% here.

D. Increased Crosstalk Effect and Decreased Propagation Delay in Graphene-Encapsulated Cu Nanointerconnects Predicted by the Proposed Multiphysics Solver

Next, to study the effect of coating graphene layers on the crosstalk, especially for cutting-edge 10-nm technology node, we analyze two parallel Cu-G nanointerconnect wires, whose geometry and discretization are illustrated in Fig. 8. We adopt similar settings as the one in Fig. 6. Each Cu interconnect, whose $W = 10$ nm, $H = 10$ nm, and $L = 10$ μm, is discretized into a uniform $10 \times 8 \times 20$ grid. In this example, we inject a current source at port 1 and port 2 in turn, whose waveform is $j_i = -(t - t_0)\exp[-((t - t_0)/\tau_s)^2]$ A/m^2,

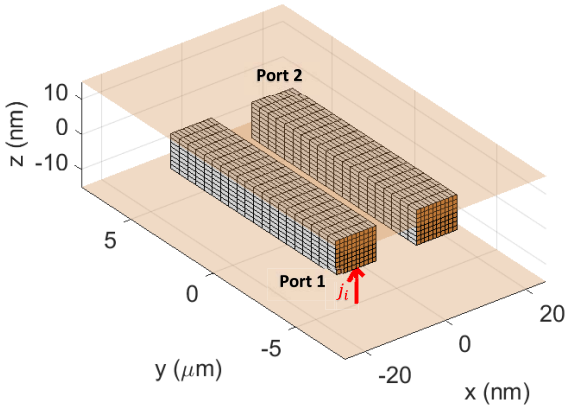

Fig. 8. Geometry and discretization of two parallel Cu-G nanointerconnects. The cross section of each nanointerconnect is 10 nm × 10 nm, much smaller than that in Fig. 6. Port voltages on ports 1 and 2 are sampled for analyzing the crosstalk S_{21}.

where $t_0 = 4\tau_s$ and $\tau_s = 2 \times 10^{-11}$ s. The pulse has a maximal signal frequency of approximately 50 GHz. Due to the small spatial feature, conventional conditionally stable methods require about 10^7 time steps to finish the simulation of Maxwell subsystem, and 10^9 time steps to simulate the Boltzmann subsystem in the window of a full pulse [29]. However, using the proposed unconditionally stable algorithm, only 200 time steps are required, where the time step is solely determined by accuracy. Furthermore, the same time step is used for simulating both Maxwell and Boltzmann subsystems. We then do an FFT on the simulated time-domain responses, from which we extract the crosstalk $|S_{21}|$ between the two ports. As can be seen in Fig. 9, the graphene coating clearly increases the crosstalk effect as compared to Cu-based counterparts.

For analyzing the propagation delay in the Cu-G nanointerconnects, we use the same structure as in Fig. 8. This time, we inject a current source of

$$j_i(t) = \begin{cases} 1.09 \times 10^{10}\ \text{A/m}^2, & 7.5\ \text{ps} < t < 57.5\ \text{ps} \\ 0, & \text{otherwise.} \end{cases}$$

The resulting port voltages, given in Fig. 10, have a ramp waveform of 50-ps transient time and 0.12-V maximum voltage, which is compatible with current complementary metal–oxide–semiconductor (CMOS) technology. The 50% propagation delay between the near-end and far-end of a single nanowire and their dependence on the length L of nanowires are listed in Table I. For the 10 nm × 10 nm thick graphene-encapsulated Cu nanointerconnects, from length $L = 5$ μm to $L = 20$ μm, the propagation delay is only 26% of the bare Cu counterparts. The result shows that Cu-G nanointerconnects have a faster data-transferring speed than that of bare Cu interconnects.

E. Comparisons Between Proposed Multiphysics Solver and Drude Model-Based Simulation in Graphene-Encapsulated Cu Nanointerconnects

Graphene has been extensively simulated via various models in the past decade. Among these models, the Drude

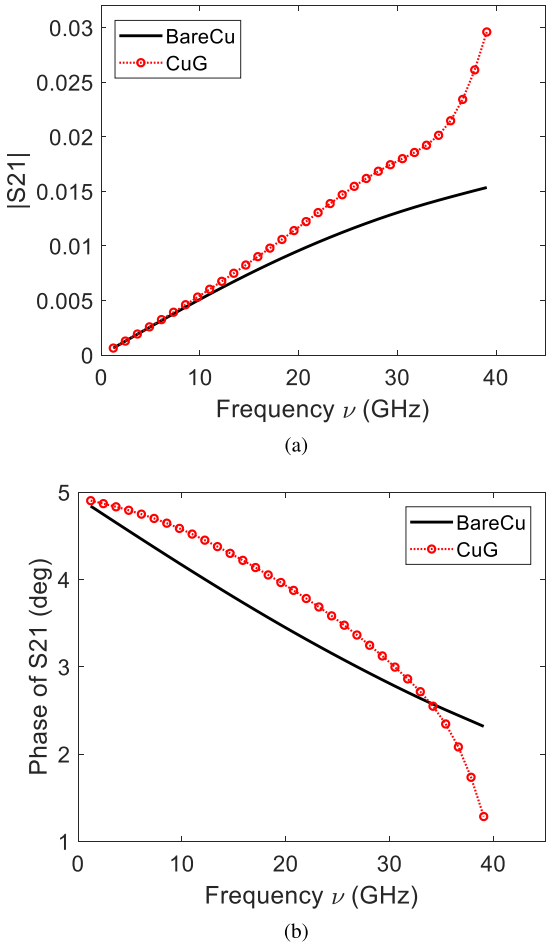

Fig. 9. Crosstalk S_{21} of the Cu-G nanointerconnects in Fig. 8. (a) Magnitude of S_{21}. (b) Phase of S_{21}.

model [13], [30]–[32], within the framework of Boltzmann transport theories, is a widely used model and has shown good accuracy in a linear regime. The analytical Drude model yields the conductivity of graphene in the frequency domain

$$\tilde{\sigma}_g(\omega) = \frac{\sigma_{dc}}{1 + j\omega\tau} \tag{27}$$

where ω is the angular frequency, τ is the relaxation time as that in the Boltzmann equation (2), and σ_{dc} is the dc conductivity of graphene. In Fig. 11, we show voltage drops predicted by the proposed multiphysics solver and the Drude model-based simulation in graphene-encapsulated Cu nanointerconnects. As can be seen, the two are very different, and the proposed solver captures physics that cannot be captured in Drude model-based simulation. The structure and parameter settings are the same as those in Fig. 8, including the same relaxation time $\tau = 20$ ps. The injected source current has a waveform of $j_i = -(t - t_0)\exp[-((t - t_0)/\tau_s)^2] \times 10^{16}$ A/m^2, where $t_0 = 4\tau_s$ and $\tau_s = 20$ ps, the maximal signal frequency of which is approximately 50 GHz. It has been shown that the relaxation time of graphene predicted by theory can vary in a wide range between 0.1 and 100 ps. However, as a modeling and simulation method, the proposed work has no restriction on the choice of material parameters. To demonstrate this

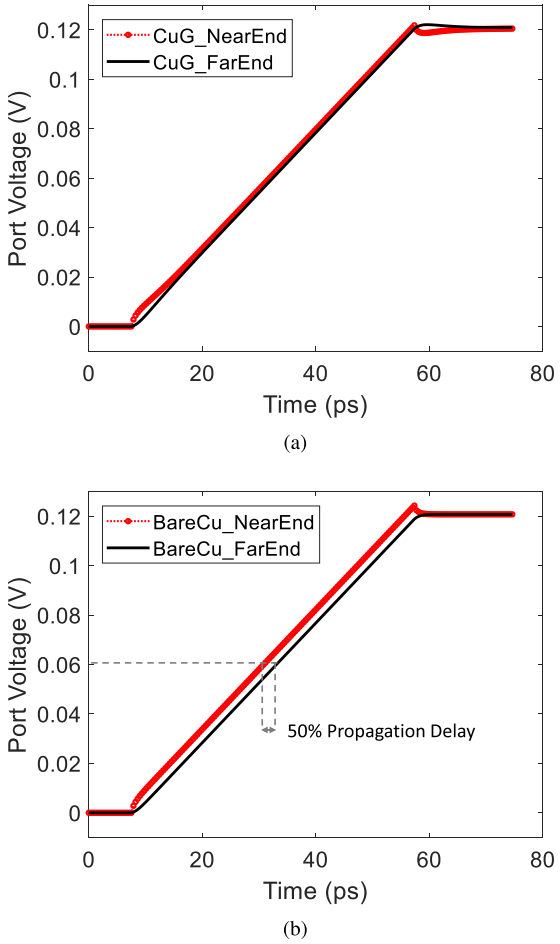

Fig. 10. Near end and far end port voltages of a single nanointerconnect. (a) Single graphene-encapsulated Cu nanointerconnect in Fig. 8. (b) Bare Cu counterparts of (a) without graphene coating.

TABLE I
PROPAGATION DELAY VERSUS LENGTH L

	Bare Cu	Cu-Graphene
$L = 20$ μm	9.0011 ps	2.2760 ps
$L = 10$ μm	2.2513 ps	0.5864 ps
$L = 5$ μm	0.5629 ps	0.1495 ps

point, we also simulated the same example using $\tau = 1$ ps, which is the relaxation time observed in many experiments. As can be seen in Fig. 11, there still exists a noticeable difference between a simplified model-based analysis and the proposed multiphysics analysis, although the difference is smaller.

From extensive numerical experiments, we have found that in structures whose size is smaller than 100 nm and when the signal frequency is comparable to the BSF of graphene, the Drude model-based simulation can miss important physical effects, while the proposed multiphysics simulation can capture it. On the other hand, for large structure sizes and lower frequencies, the two simulations can generate the same results. Due to limited space, the details of this part are not reported here, but they can be found in [33].

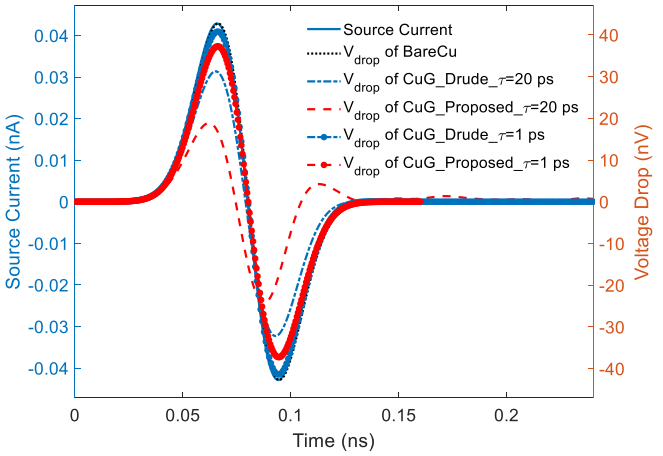

Fig. 11. Time-domain voltage drop (labeled to the right) along the single graphene-encapsulated Cu nanointerconnect in Fig. 8. The Gaussian derivative source current is plotted in solid line and labeled to the left.

V. CONCLUSION

In this article, we propose a multiphysics model for general 3-D Cu-G hybrid nanointerconnects via cosimulating in time-domain Maxwell's equations, Boltzmann equation under relaxation time approximation, and the linear dispersion of graphene. We also develop an unconditionally stable simulation algorithm for the proposed multiphysics model, allowing for the use of an arbitrarily large time step irrespective of the extremely small space step for simulating nanointerconnects. Numerical experiments and their comparisons with measurements validate the accuracy and efficiency of the proposed multiphysics modeling algorithm. From the simulated full-wave response in time domain, many essential parameters of Cu-G nanointerconnects, including electrical conductivity, crosstalk effect, and propagation delay, can be easily evaluated. In the future, more physics effects, such as the intraband transition in graphene and the surface scattering at the Cu-G interface, can be included to further enrich the multiphysics model and enhance the prediction power.

REFERENCES

[1] R. C. Munoz and C. Arenas, "Size effects and charge transport in metals: Quantum theory of the resistivity of nanometric metallic structures arising from electron scattering by grain boundaries and by rough surfaces," *Appl. Phys. Rev.*, vol. 4, no. 1, 2017, Art. no. 011102.

[2] D. Josell, S. H. Brongersma, and Z. Tőkei, "Size-dependent resistivity in nanoscale interconnects," *Annu. Rev. Mater. Res.*, vol. 39, pp. 231–254, Aug. 2009.

[3] R. Mehta, S. Chugh, and Z. Chen, "Enhanced electrical and thermal conduction in graphene-encapsulated copper nanowires," *Nano Lett.*, vol. 15, no. 3, pp. 2024–2030, Mar. 2015.

[4] C. G. Kang *et al.*, "Effects of multi-layer graphene capping on Cu interconnects," *Nanotechnol.*, vol. 24, no. 11, 2013, Art. no. 115707.

[5] P. Goli, H. Ning, X. Li, C. Y. Lu, K. S. Novoselov, and A. A. Balandin, "Thermal properties of graphene–copper–graphene heterogeneous films," *Nano Lett.*, vol. 14, no. 3, pp. 1497–1503, 2014.

[6] N. T. Cuong and S. Okada, "Suppression of conductivity deterioration of copper thin films by coating with atomic-layer materials," *Appl. Phys. Lett.*, vol. 110, no. 13, p. 131601, 2017.

[7] G. W. Hanson, "Dyadic Green's functions and guided surface waves for a surface conductivity model of graphene," *J. Appl. Phys.*, vol. 103, no. 6, 2008, Art. no. 064302.

[8] A. Naeemi and J. D. Meindl, "Compact physics-based circuit models for graphene nanoribbon interconnects," *IEEE Trans. Electron Devices*, vol. 56, no. 9, pp. 1822–1833, Sep. 2009.
[9] A. G. D. Aloia, W.-S. Zhao, G. Wang, and W.-Y. Yin, "Near-field radiated from carbon nanotube and graphene-based nanointerconnects," *IEEE Trans. Electromagn. Compat.*, vol. 59, no. 2, pp. 646–653, Jan. 2017.
[10] V. Nayyeri, M. Soleimani, and O. M. Ramahi, "Modeling graphene in the finite-difference time-domain method using a surface boundary condition," *IEEE Trans. Antennas Propag.*, vol. 61, no. 8, pp. 4176–4182, Aug. 2013.
[11] R. M. S. D. Oliveira, N. R. N. M. Rodrigues, and V. Dmitriev, "FDTD formulation for graphene modeling based on piecewise linear recursive convolution and thin material sheets techniques," *IEEE Antennas Wireless Propag. Lett.*, vol. 14, pp. 767–770, 2015.
[12] A. Vakil and N. Engheta, "Transformation optics using graphene," *Science*, vol. 332, no. 6035, pp. 1291–1294, 2011.
[13] D. Sarkar, C. Xu, H. Li, and K. Banerjee, "High-frequency behavior of graphene-based interconnects—Part I: Impedance modeling," *IEEE Trans. Electron Devices*, vol. 58, no. 3, pp. 843–852, Mar. 2011.
[14] C. Berger *et al.*, "Electronic confinement and coherence in patterned epitaxial graphene," *Science*, vol. 312, no. 5777, pp. 1191–1196, Apr. 2006.
[15] E. H. Hwang and S. D. Sarma, "Single-particle relaxation time versus transport scattering time in a two-dimensional graphene layer," *Phys. Rev. B, Condens. Matter*, vol. 77, no. 19, May 2008, Art. no. 195412.
[16] S. Sun and D. Jiao, "Multiphysics modeling and simulation of 3-D Cu-graphene hybrid nano-interconnects," in *Proc. IEEE MTT-S Int. Conf. Numer. Electromagn. Multiphys. Modeling Optim. (NEMO)*, May 2019, pp. 1–4.
[17] C. Kittel, *Introduction to Solid State Physics*, 8th ed. Hoboken, NJ, USA: Wiley, 2005.
[18] H. Peng *et al.*, "Substrate doping effect and unusually large angle van hove singularity evolution in twisted bi- and multilayer graphene," *Adv. Mater.*, vol. 29, no. 27, 2017, Art. no. 1606741.
[19] J. Yan and D. Jiao, "Time-domain method having a naturally diagonal mass matrix independent of element shape for general electromagnetic analysis—2-D formulations," *IEEE Trans. Antennas Propag.*, vol. 65, no. 3, pp. 1202–1214, Jan. 2017.
[20] J. Yan and D. Jiao, "Fast explicit and unconditionally stable FDTD method for electromagnetic analysis," *IEEE Trans. Microw. Theory Techn.*, vol. 65, no. 8, pp. 2698–2710, Aug. 2017.
[21] C. Jungemann and B. Meinerzhagen, "Analysis of the stochastic error of stationary Monte Carlo device simulations," *IEEE Trans. Electron Devices*, vol. 48, no. 5, pp. 985–992, May 2001.
[22] P. W. Rambo and J. Denavit, "Time stability of Monte Carlo device simulation," *IEEE Trans. Comput.-Aided Design Integr. Circuits Syst.*, vol. 12, no. 11, pp. 1734–1741, Nov. 1993.
[23] L. Varani, L. Reggiani, T. Kuhn, T. Gonzalez, and D. Pardo, "Microscopic simulation of electronic noise in semiconductor materials and devices," *IEEE Trans. Electron Devices*, vol. 41, no. 11, pp. 1916–1925, Nov. 1994.
[24] S.-M. Hong, A.-T. Pham, and C. Jungemann, *Deterministic Solvers for the Boltzmann Transport Equation*. Vienna, Austria: Springer, 2011. [Online]. Available: https://link.springer.com/book/10.1007%2F978-3-7091-0778-2#about
[25] K. Zhao, S. Hong, C. Jungemann, and R. Han, "Stable implementation of a deterministic multi-subband boltzmann solver for silicon double-gate nMOSFETs," in *Proc. Int. Conf. Simulation Semiconductor Processes Devices*, Sep. 2010, pp. 303–306.
[26] R. J. LeVeque, *Finite Difference Methods for Ordinary and Partial Differential Equations*. Philadelphia, PA, USA: SIAM, 2007.
[27] J. G. Maloney and G. S. Smith, "The efficient modeling of thin material sheets in the finite-difference time-domain (FDTD) method," *IEEE Trans. Antennas Propag.*, vol. 40, no. 3, pp. 323–330, Mar. 1992.
[28] M. J. Kobrinsky, S. Chakravarty, D. Jiao, M. C. Harmes, S. List, and M. Mazumder, "Experimental validation of crosstalk simulations for on-chip interconnects using S-parameters," *IEEE Trans. Adv. Packag.*, vol. 28, no. 1, pp. 57–62, Feb. 2005.
[29] S. Sun and D. Jiao, "Multiphysics simulation of high-speed graphene-based interconnects in time domain," in *Proc. IEEE Int. Symp. Antennas Propag.*, Jul. 2018, pp. 1169–1170.
[30] R. Wang, X.-G. Ren, Z. Yan, L.-J. Jiang, W. E. I. Sha, and G.-C. Shan, "Graphene based functional devices: A short review," *Frontiers Phys.*, vol. 14, no. 1, p. 13603, Oct. 2018.
[31] B. Sensale-Rodriguez *et al.*, "Broadband graphene terahertz modulators enabled by intraband transitions," *Nature Commun.*, vol. 3, p. 780, Apr. 2012.
[32] J. Horng *et al.*, "Drude conductivity of Dirac fermions in graphene," *Phys. Rev. B, Condens. Matter*, vol. 83, Apr. 2011, Art. no. 165113.
[33] S. Sun and D. Jiao, "First-principles based multiphysics modeling and simulation of on-chip cu-graphene hybrid nano-interconnects in comparison with simplified model based analysis," *IEEE J. Multiscale Multiphys. Comput. Techn.*, to be published.

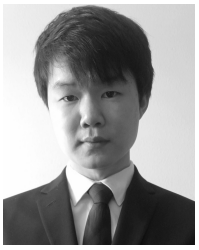

Shuzhan Sun (GS'18) received the B.S. degree in physics from the School of Special Class for the Gifted Young, University of Science and Technology of China, Hefei, China, in 2016. He is currently pursuing the Ph.D. degree in electrical and computer engineering (with a minor M.S. degree in physics in 2018) in the On-Chip Electromagnetics Group, Purdue University, West Lafayette, IN, USA.

His current research focuses on simulating next-generation Cu-graphene hybrid nanointerconnects and developing novel electromagnetic algorithms for large-scale simulation.

Mr. Sun received the Best Student Paper Award Finalist at the IEEE International Symposium on Antennas and Propagation in 2019.

Dan Jiao (M'02–SM'06–F'16) received the Ph.D. degree in electrical engineering from the University of Illinois at Urbana–Champaign, Champaign, IL, USA, in 2001.

She then worked at the Technology Computer-Aided Design (CAD) Division, Intel Corporation, Santa Clara, CA, USA, until September 2005, as a Senior CAD Engineer, a Staff Engineer, and a Senior Staff Engineer. In September 2005, she joined Purdue University, West Lafayette, IN, USA, as an Assistant Professor with the School of Electrical and Computer Engineering, where she is currently a Professor. She has authored three book chapters and over 260 articles in refereed journals and international conferences. Her current research interests include computational electromagnetics, high-frequency digital, analog, mixed-signal, and RF integrated circuit (IC) design and analysis, high-performance VLSI CAD, modeling of microscale and nanoscale circuits, applied electromagnetics, fast and high-capacity numerical methods, fast time-domain analysis, scattering and antenna analysis, RF, microwave, and millimeter-wave circuits, wireless communications, and bio-electromagnetics.

Dr. Jiao received the 2013 S. A. Schelkunoff Prize Paper Award from the IEEE Antennas and Propagation Society, which was recognized as the best paper published in the IEEE TRANSACTIONS ON ANTENNAS AND PROPAGATION during the previous year. She was among the 21 women faculty selected across the country as the 2014-2015 Fellow of Executive Leadership in Academic Technology and Engineering (ELATE) at Drexel, a national leadership program for women in the academic STEM fields. She has been named as the University Faculty Scholar by Purdue University since 2013. She was among the 85 engineers selected throughout the nation for the National Academy of Engineering's 2011 U.S. Frontiers of Engineering Symposium. She was a recipient of the 2010 Ruth and Joel Spira Outstanding Teaching Award, the 2008 National Science Foundation (NSF) CAREER Award, the 2006 Jack and Cathie Kozik Faculty Start-up Award, for which she was recognized as an Outstanding New Faculty Member of the School of Electrical and Computer Engineering, Purdue University, the 2006 Office of Naval Research (ONR) Award through the Young Investigator Program, the 2004 Best Paper Award presented at the Intel Corporation's annual corporate-wide technology conference (Design and Test Technology Conference) for her work on generic broadband model of high-speed circuits, the 2003 Intel Corporation's Logic Technology Development (LTD) Divisional Achievement Award, the Intel Corporation's Technology CAD Divisional Achievement Award, the 2002 Intel Corporation's Components Research the Intel Hero Award (Intel-wide she was the tenth recipient), the Intel Corporation's LTD Team Quality Award, and the 2000 Raj Mittra Outstanding Research Award from the University of Illinois at Urbana–Champaign. She has served as a reviewer for many IEEE journals and conferences. She is an Associate Editor of the IEEE TRANSACTIONS ON COMPONENTS, PACKAGING, AND MANUFACTURING TECHNOLOGY and the IEEE JOURNAL ON MULTISCALE AND MULTIPHYSICS COMPUTATIONAL TECHNIQUES.